Sensors and Materials, Vol. 37, No. 3 (2025) 943–953
MYU Tokyo

S & M 3967

Microfabrication of Black Ge by SF_6/O_2- and C_4F_8-based Deep Reactive Ion Etching

Mie Tohnishi,[1*] Sachiko Matsushita,[2,3] and Akihiro Matsutani[1]

[1]Research Infrastructure Management Center, Institute of Science Tokyo,
R2-3, 4259 Nagatsuta-cho, Midori-ku, Yokohama, Kanagawa 226-8503, Japan
[2]Department of Materials Science and Engineering, Institute of Science Tokyo,
J2-48, 4259 Nagatsuta-cho, Midori-ku, Yokohama, Kanagawa 226-8503, Japan
[3]elleThalmo, Ltd., INDEST 3F, Institute of Science Tokyo, 3-3-6 Shibaura, Minato-ku, Tokyo 108-0023, Japan

(Received October 21, 2024; accepted January 22, 2025)

Keywords: microfabrication, black Ge, deep RIE, regular reflectance, emissivity

We fabricated black Ge with numerous needlelike microstructures by SF_6/O_2- and C_4F_8-based deep reactive ion etching and measured the regular reflectance in the ultraviolet-to-near-infrared range, thermal radiation properties, and electrical resistance for electrode applications. The regular reflectance of black Ge was very low in the range of 250 nm–2.5 µm. The emissivity of the black Ge surface was observed to be the same as that of a carbon plate. We found that the scallops on the sidewalls of the microstructures also contributed to the low reflectance. Furthermore, the black Ge electrode had a lower resistance than a planar Ge electrode. The black Ge electrode, which has an increased surface area of Ge with numerous needlelike microstructures, has high emissivity, antireflectivity and low resistance, and we consider that it is useful for application to device fabrication utilizing these properties.

1. Introduction

Renewable energy is a particularly active field of research today, which is pursued to meet the rising energy needs of society and to solve global energy problems. The use of renewable energies, such as solar, wind, tidal, and thermal energies, has recently attracted considerable attention[1–4] owing to both environmental and resource issues. Among these renewable energies, we focus on thermal energy. Efficient and low-cost thermal energy-harvesting systems such as semiconductor-sensitized thermal cells (STCs)[5–13] have been proposed as a new thermal energy conversion technology based on dye-sensitized solar cells.[14,15] STCs generate electricity by the redox reactions of electrolyte ions with thermally excited carriers in semiconductors. Germanium (Ge) is often used as a semiconductor because it has a band gap of about 0.7 eV and generates a large amount of thermally excited charge even at relatively low temperatures around 80 ℃. The Ge–STC shows its stable battery characteristics owing to the polymer electrolyte including CuCl and $CuCl_2$ as electrolyte ions. The energy conversion efficiency of STCs has been reported to be 9.2% at approximately 90 ℃.[7] Since STCs generate electricity through

*Corresponding author: e-mail: tohnishi.m.ab@m.titech.ac.jp
https://doi.org/10.18494/SAM5404

ISSN 0914-4935 © MYU K.K.
https://myukk.org/

chemical reactions at the interface of the electrode and electrolyte, having a high specific surface area for the electrode enhances the current acquisition. Additionally, properties such as high emissivity and antireflection due to increased surface area help confine thermal energy within the semiconductor electrode, leading to the efficient generation of thermally excited carriers in the semiconductor. The fabrication of microstructures on the electrode surface is an effective method of increasing the surface area. The fabrication of a black Si structure whose surface is covered with numerous microstructures is one method of increasing the surface area.[16–21] The microstructures on the surface of black Si are many microneedles with high aspect ratios. Similarly, covering the Ge surface with numerous microstructures is also an effective method of increasing the surface area. There have been examples of black Ge fabrication using gases such as SF_6/O_2, SF_6/C_4F_8, Cl_2, and SF_6/CHF_3.[22–26] The fabrication of high-aspect-ratio needlelike structures by etching is expected to be achieved under similar process conditions as the etching of narrow trenches with high aspect ratios. Previously, we reported a method of etching narrow trench structures in Si by SF_6/O_2- and C_4F_8-based deep reactive ion etching.[22] We expect that the same manner can be demonstrated for the microfabrication of black Ge. There have been several reports on the reflectivity of such black Ge measured by the total reflection, but since black Ge has many high aspect ratio beam structures, it is necessary to measure the regular reflectivity as well. However, there are few reports on the positive reflectance of black Ge.

In this study, we report the fabrication of black Ge consisting of numerous needlelike microstructures with scalloped sidewalls by SF_6/O_2- and C_4F_8-based deep reactive ion etching (RIE). We measured the emissivity of black Ge. Furthermore, the scallop depth and chemical composition of the etched sidewalls were analyzed by atomic force microscopy (AFM) and energy-dispersive X-ray spectroscopy (EDX), respectively. We also measured the reflectance of black Ge, the angle dependence of the regular reflectance of black Ge in the range of 250 nm–2.5 µm, and the dependence of the scallop depth of the microstructure sidewalls. Finally, to investigate the electrical properties of black Ge, an experiment was performed using an electrolyte and a platinum.

2. Experimental Methods

Figure 1 shows a schematic of the deep RIE setup (SPP MUC21-HRMX: chamber size, ϕ340 mm; electrode size, ϕ200 mm) equipped with a switching system with SF_6 and O_2 as the etching gases and C_4F_8 as the passivation gas used in this experiment. A 1-mm-thick n-type Ge (111) substrate was used as a sample, which was placed on a ϕ200 mm aluminum tray. The microstructure of the sample fabricated by deep RIE was observed by SEM (Hitachi High-Tech FlexSEM1000II) and AFM (Hitachi High-Tech AFM500II). The chemical composition of the microstructures was analyzed by EDX (OXFORD Instruments AZtechOne). Infrared images of the samples were taken using an infrared thermographic camera (FLIR THI-501AJ). The reflectance of the samples was measured using a spectrophotometer (SHIMADZU SolidSpec 3700DUV). To smooth the scallops of the sidewall of microstructures of black Ge for comparison, O_2 plasma treatment was performed with RIE (SAMCO RIE-10NR).

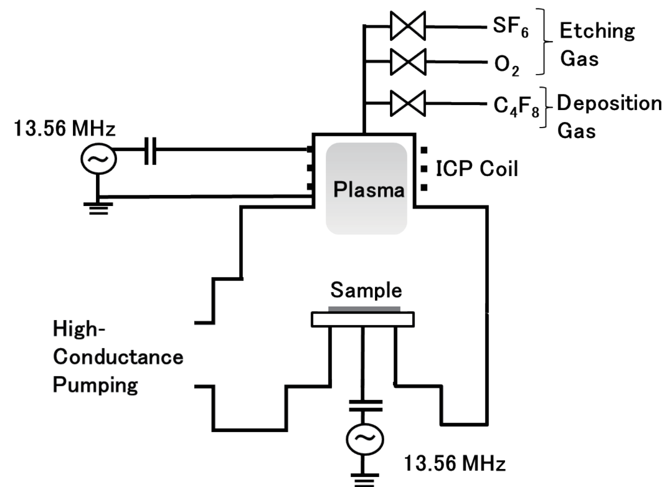

Fig. 1. Schematic of Deep-RIE to fabrication of black Ge.

3. Results and Discussion

3.1 Microfabrication and analysis of microstructure surface of black Ge

To fabricate black Ge microstructures by dry etching, numerous micromasks are required, and it is difficult to fabricate micromasks for large areas by electron beam lithography. However, it is easy to fabricate micromasks using fluorocarbons generated in the plasma used in the deposition process. In deep RIE, the deposition of the passivation film and etching are switched repeatedly. In the first cycle, C_4F_8 plasma forms a fluorocarbon polymer as a passivation layer. In the subsequent etching step, the polymer is removed by SF_6/O_2 plasma and the Ge surface is isotropically etched. The remaining polymer tends to form into several clusters. These clusters become micromasks for the formation of microstructures. Needlelike microstructures are formed by repeated switching between deposition and etching. The deep RIE conditions for black Ge fabrication are shown in Table 1.

Figure 2(a) shows a top-view photograph of samples at different process times. The Ge surface lost its luster after 5 min and became gray after 15 min and almost black after 30 min. The Ge surface changed to gray again after 45 min. Figure 2(b) shows 45°-tilted SEM images of the microstructures on the Ge surface at different process times. The heights of the microstructures were estimated to be 7 µm after 5 min, 20 µm after 15 min, and 40 µm after 30 min. The microstructures were completely removed after 45 min. Figure 2(c) shows the microstructure height and etching depth as functions of process time. Owing to mask erosion in the etching step, the microstructure height was smaller than the etching depth.

Next, the emissivity of black Ge was investigated by infrared thermography. Infrared images were taken during heating on a hot plate at 90 °C. In this image, the emissivity ε was set to 0.95. The samples were 1-mm-thick ϕ15 mm Ge substrates cut into quarters, planar Ge ($\varepsilon = 0.6$), black Ge, and black body tape ($\varepsilon = 0.95$) on planar Ge. The samples were placed on a ϕ120 mm carbon

Table 1
Summary of deep RIE conditions.

Processing step	Gas	Flow rate (sccm)	Pressure (Pa)	ICP-RF (W)	Bias-RF (W)	Cycle time (s)
Deposition	C_4F_8	90	2	1500	20	5
Etching	SF_6/O_2	200/20	4	2200	40	5

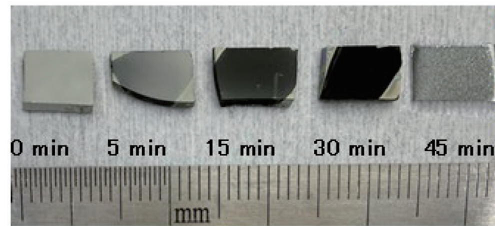

(a)

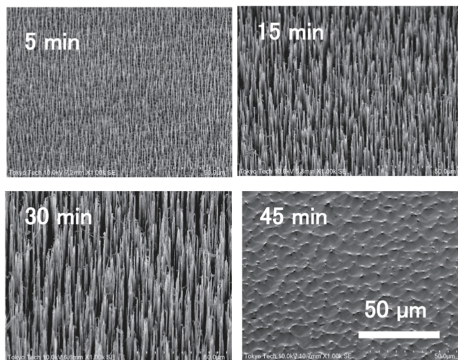

(b)

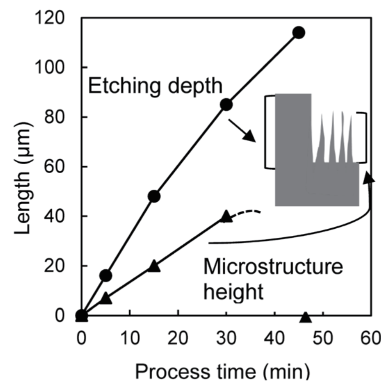

(c)

Fig. 2. (Color online) (a) Top-view photograph of samples at different process times. (b) 45°-tilted SEM images of samples at different process times. (c) Etching depth and microstructure height as functions of process time.

plate (ε = 0.85). Figure 3 shows an infrared image obtained when the temperature of the black body tape was 85.8 ℃. The temperatures of all the samples should be the same; however, the surface of planar Ge was observed to exhibit the lowest temperature. The emissivity of black Ge fabricated by deep RIE was higher than that of planar Ge. It is considered that the displayed temperatures of these samples indicate a difference in emissivity. As can be seen from Fig. 3, the emissivity of black Ge is about the same as that of the carbon plate. Therefore, we believe that the emissivity can be increased by the fabrication of a microstructure as black Ge.

Figure 4 shows the AFM image and line profile of the sidewalls of the microstructures. The surface of the microstructures has a regularly scalloped figure. In this experiment, the scallop depth was about 200 nm and the scallop pitch was about 220 nm. The scallop depth was approximately equal to the etching depth per cycle, and the sidewalls were also isotropically etched. Scallops are formed on the sidewalls of the microstructures as a result of the switching between deposition and isotropic etching.

We analyzed the chemical composition of the sidewalls of the microstructure by EDX. To simplify the measurements, EDX analysis was performed on a broken microstructure. The

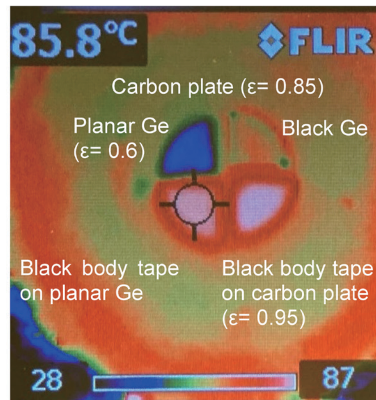

Fig. 3. (Color online) Infrared image of samples on carbon hot plate.

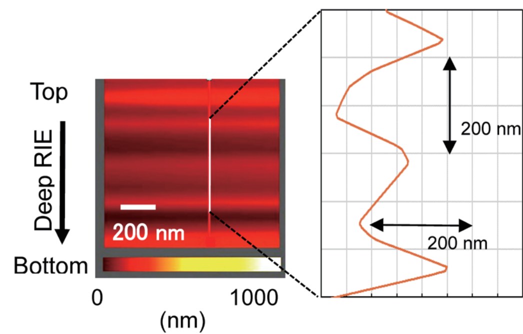

Fig. 4. (Color online) AFM image and line profile of the scallop of the sidewalls of the microstructures.

analysis point of the microstructure is shown in Fig. 5(a). The microstructure was about 2 μm in diameter except at its tip. As shown in Fig. 5(b), when the acceleration voltage was set to 10 kV and the spot size was about 10 nm, the X-ray generation region in this EDX analysis was estimated to be 0.7 μm from Castaing's equation.[27] We analyzed the atomic ratios of Ge, F, C and O. The atomic ratios of F and O were below the limit of measurement. The atomic ratios of C were 34, 29, and 25% at measurement points 10 μm (upper), 20 μm (middle), and 30 μm (bottom), respectively, from the tip of the microstructure. The trend for the carbon-rich surface was the same as that for the sidewalls of a high-aspect-ratio Si narrow trench in our previous report.[22] We found that the carbon-rich surface on scallops is effective as a passivation film to protect the sidewalls from etching by fluorine radicals for the formation of a high-aspect-ratio microstructure.

3.2 Measurement of reflectance of black Ge

The reflectance of the black Ge surface was measured in the UV-to-NIR (250 nm–2.5 μm) region using photomultiplier tubes (250–850 nm), InGaAs cells (850 nm–1.65 μm), and Pbs cells (1.65–2.5 μm) as detectors. Data at around the wavelength of 850 nm were excluded because the correct reflectance cannot be measured owing to the switching of the detector. The total reflectance spectra of black Ge and planar Ge are shown in Fig. 6(a). Up to a wavelength of 1.4 μm, the reflectivity was around 2%, increasing to only 20% at 1.8 μm. The total reflectivity increased above 1.55 μm. Figure 6(b) shows the regular reflectance spectra of black Ge and planar Ge. The angle of the incident light was 5°. The regular reflectance of the fabricated black Ge was extremely low in the UV-to-near-infrared region up to a wavelength of 2.5 μm. The reflectivity of black Ge was dominated by light scattering and light absorption within the microstructures. There was no significant difference between the total reflectance and regular reflectance of planar Ge. In the measurement of the total reflectance, the reflectance included diffuse reflection, i.e., the reflectance of the side of the needlelike microstructure was also

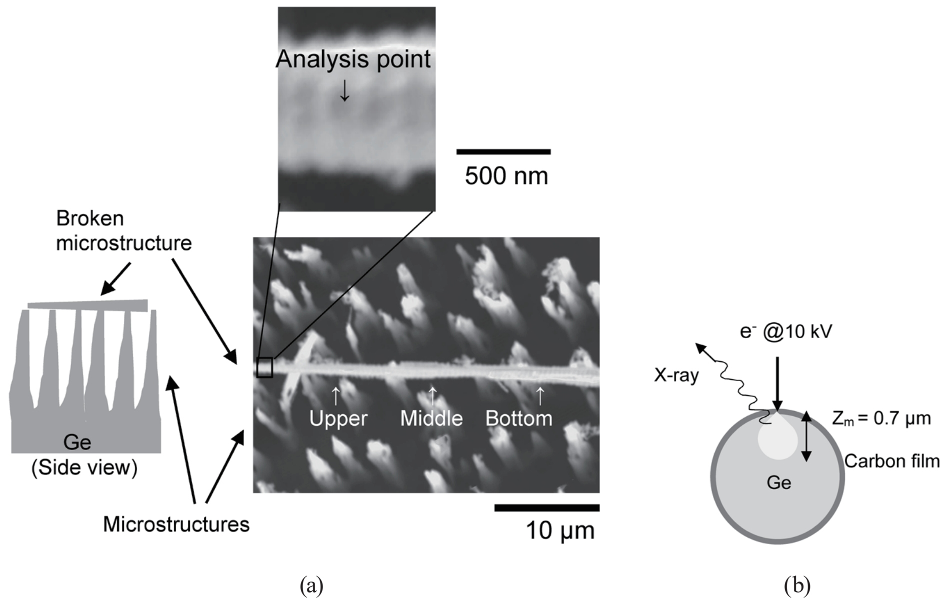

Fig. 5. (a) Point of microstructure analyzed by EDX (top view). (b) Schematic of X-ray generation area of the cross section of a microstructure.

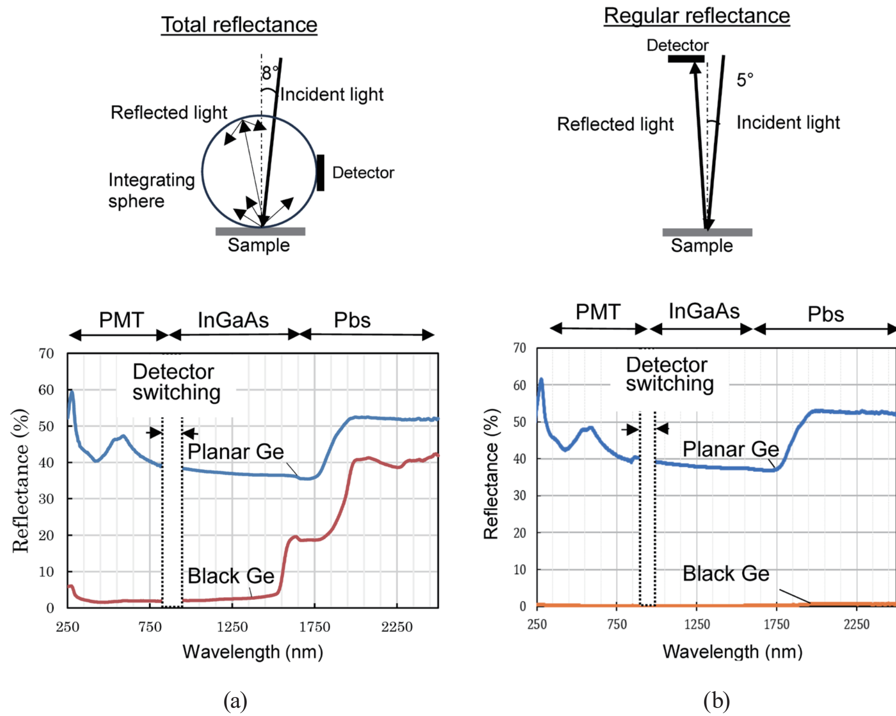

Fig. 6. (Color online) (a) Total and (b) regular reflectance spectra of black Ge and planar Ge.

measured. On the other hand, in the regular reflectance measurement, the reflectance seen from the front of the needlelike microstructure was measured and considered to be suitable for evaluating the reflectance of black Ge.

By regular reflection measurements, the angular dependence of the reflectance of the needlelike microstructure of black Ge can also be measured. Figure 7(a) shows the incident angle dependence of the black Ge reflectance. Measurements were conducted at incident angles of 5, 15, and 30°. When the incident angle increased, the reflectance decreased. The measured reflectance was below 1% in the wavelength range lower than the bandgap energy. It is deduced that the reflectance increased owing to the light scattering in the wavelength range of above 1550 nm.[23] Figure 7(b) shows the schematic needlelike microstructures of the black Ge surface. The shape of the microstructure is tapered, and its tip is thin like a needle. Figure 7(c) shows a schematic of the model of light traveling in the scallops on the sidewall of the needlelike microstructure. In Fig. 7(c), light with a small incident angle of 5° is reflected at the scallop tip and reaches the detector, whereas light with a large incident angle of 30° is reflected at the scallop tip and travels inside the scallop and cannot reach the detector. In other words, the reflectance is expected to be lower at the angle of incidence of light of 30° to the scallops of black Ge.

Next, we investigated the dependence of the reflectance on the scallop depth of the sidewalls of the microstructures. As mentioned in Sect. 3.1, the sidewalls of the microstructures are covered with carbon. Therefore, we considered that the scallop depth of the sidewalls of the microstructures can be made smaller by O_2 plasma treatment.[28] O_2 plasma treatment was carried out in the RIE system. Figure 8(a) shows SEM images of black Ge obtained before and after 10 min of O_2 plasma treatment. It can be seen that the sidewalls of the microstructures were smoothed by O_2 plasma treatment. Figure 8(b) shows the AFM line profile of the sidewalls of the

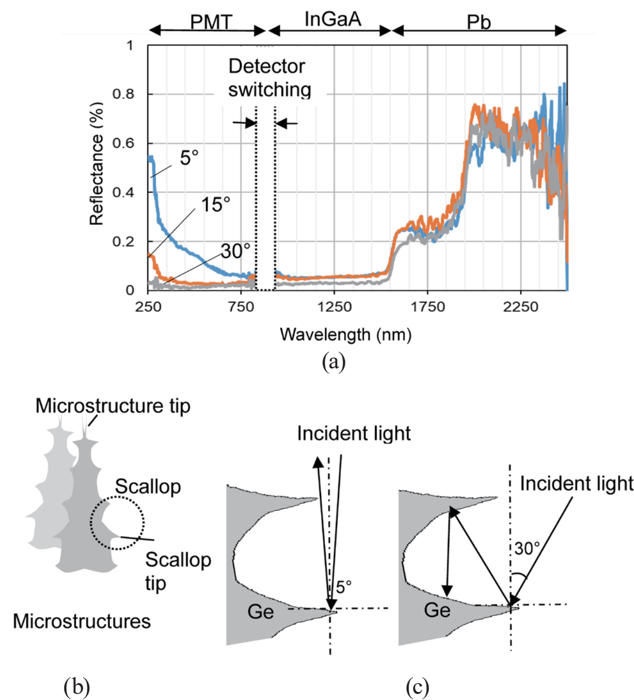

Fig. 7. (Color online) (a) Angular dependence of black Ge reflectance. (b) Schematic of microstructures. (c) Model of angular dependence of reflection on the scallop.

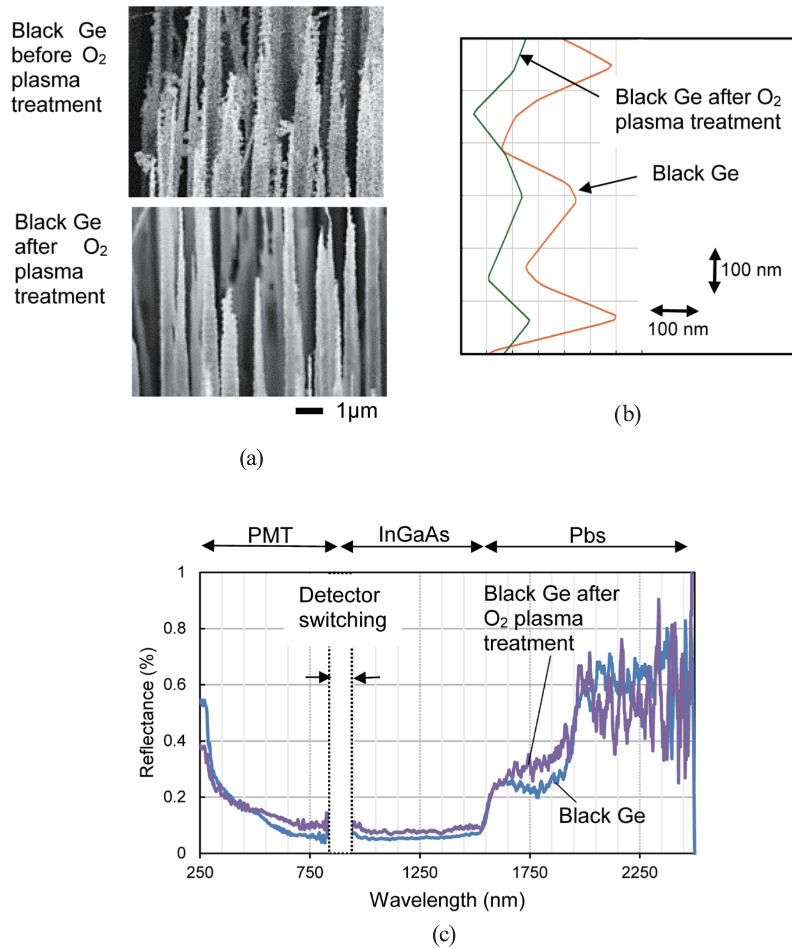

Fig. 8. (Color online) (a) SEM images of black Ge obtained before and after O_2 plasma treatment. (b) AFM line profiles of the scallops of the sidewall of black Ge obtained before and after O_2 plasma treatment. (c) Reflectance spectra of black Ge obtained before and after O_2 plasma treatment.

microstructures smoothed by O_2 plasma treatment. The depth of the scallop of the sidewalls of the microstructures was 200 nm, which was reduced to approximately 100 nm by O_2 plasma treatment. Figure 8(c) shows the reflectance spectra of black Ge obtained before and after O_2 plasma treatment. The reflectance of black Ge with O_2 plasma treatment was slightly higher than that without the treatment. We believe that scallops of the sidewalls of microstructures also contribute to the decrease in the reflectance of black Ge.

3.3 Measurement of resistance of black Ge electrode

Finally, to investigate the electrical properties of black Ge, the electrical resistance of black Ge was compared with that of planar Ge using an electrolyte and Pt. Figure 9(a) shows a photograph of the Ge and Pt electrodes used in this experiment. The Ge electrodes were fabricated on each surface of a ϕ35 mm Ge substrate with a thickness of 1.5 mm cut into four

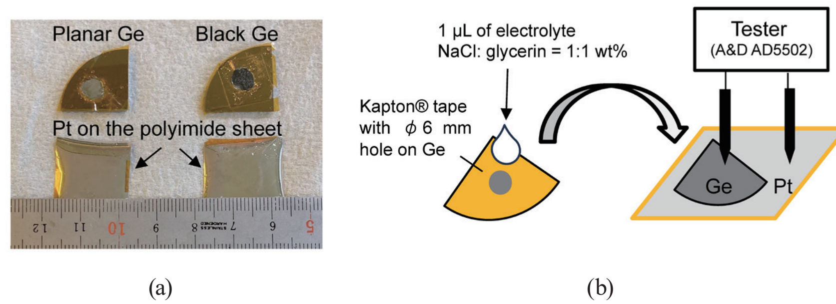

(a) (b)

Fig. 9. (Color online) (a) Top view of Ge and Pt electrodes on the polyimide sheet. (b) Schematic of the resistance measurement of Ge and Pt cells.

Table 2
Comparison of resistances of black Ge electrode and planar Ge electrode.

Electrode	Planar Ge	Black Ge
Resistance (kΩ)	82	58

pieces. Planar Ge was fabricated by covering the Ge substrate with Kapton® tape (t = 50 μm) with a ϕ6 mm hole. The black Ge electrode was fabricated by covering the Ge substrate with Kapton tape with a ϕ6 mm hole and etching it by deep RIE. As mentioned above, the surface of black Ge after deep RIE is carbon-rich, and black Ge immediately after etching was used in this experiment. The Pt electrode was deposited by sputtering on a 50-μm-thick polyimide sheet. Figure 9(b) shows a schematic of the electrical resistance measurement setup using the samples in Fig. 9(a). The electrolyte was made by mixing NaCl and glycerin in 1:1 ratio. The electrolyte was filled into the hole of the Kapton tape on the Ge electrode, and it was sandwiched between the Ge electrode and the Pt electrode. The electrical resistance between the Ge electrode and the Pt electrode was measured by applying a tester pin. Table 2 shows the electrical resistance of this measurement system when the black and planar Ge electrodes were used. The resistance when the black Ge electrode was used was about 30% lower than that when the planar Ge electrode was used. This reduction in electrical resistance is considered to be due to the increase in the area of Ge in contact with the electrolyte.(29) However, this reduction in resistance may not be solely due to the effect of increasing the surface area, since other factors, such as the difference in electrical conductivity between Ge and carbon, may also be involved. We would like to study further details in the future.

4. Conclusions

We demonstrated the microfabrication of black Ge by SF_6/O_2- and C_4F_8-based deep RIE. The surface of Ge was etched by deep RIE to numerous needlelike microstructures that had scallops on the sidewall. In the measurement with an infrared thermometer, the emissivity of the surface of black Ge was found to be higher than that of planar Ge and the same as that of a carbon plate. In addition, the regular reflectance of black Ge was extremely low from the ultraviolet region to the near-infrared region. The shape of the scallop of the sidewall of the microstructures of black

Ge also contributed to the low reflectivity. Also, the electrical resistance of the black Ge electrode was about 30% lower than that of the planar Ge electrode. From these experiments, we believe that black Ge with high emissivity, antireflectivity, and low resistance is useful for improving the performance of electrical and thermal devices such as STCs.

Acknowledgments

This research was supported by a Grant-in-Aid for Scientific Research (B) (21H02041) and by the Ministry of Education, Culture, Sports, Science and Technology of Japan (MEXT) under the Advanced Research Infrastructure Sharing Promotion Program (Core Facility Construction Support Program JPMXS0440200021).

References

1 M. Matsumoto, Y. Wada, T. Kitamura, K. Shigaki, T. Inoue, M. Ikeda, and S. Yanagida: Bull. Chem. Soc. Jpn. **74** (2001) 387.
2 S. C. Pryor, R. J. Barthelmie, M. S. Bukovsky, L. R. Leung, and K. Sakaguchi: Nat. Rev. Earth Environ. **1** (2020) 627.
3 A. Roberts, B. Thomas, P. Sewell, Z. Khan, S. Balmain, and J. Gillman: J. Ocean Eng. Mar. Energy **2** (2016) 227.
4 A. Chapman, E. Ertekin, M. Kubota, A. Nagao, K. Bertsch, A. Macadre, T. Tsuchiyama, T. Masamura, S. Takaki, R. Komoda, M. Dadfarnia, B. Somerday, A. T. Staykov, J. Sugimura, Y. Sawae, T. Morita, H. Tanaka, K. Yagi, V. Niste, P. Saravanan, S. Onitsuka, K.-S. Yoon, S. Ogo, T. Matsushima, G. Tumen-Ulzii, D. Klotz, D. H. Nguyen, G. Harrington, C. Adachi, H. Matsumoto, L. Kwati, Y. Takahashi, N. Kosem, T. Ishihara, M. Yamauchi, B. B. Saha, M. A. Islam, J. Miyawaki, H. Sivasankaran, M. Kohno, S. Fujikawa, R. Selyanchyn, T. Tsuji, Y. Higashi, R. Kirchheim, and P. Sofronis: Bull. Chem. Soc. Jpn. **95** (2022) 73.
5 S. Matsushita, T Araki, B. Mei, S. Sugawara, Y. Inagawa, J. Nishiyama, T. Isobe, and A. Nakajima: J. Mater. Chem. A **7** (2019) 18249.
6 Y. Inagawa, T. Isobe, A. Nakajima, and S. Matsushita: J. Phys. Chem. C **123** (2019) 12135.
7 S. Matsushita, S. Sugawara, T. Isobe, and A. Nakajima: ACS Appl. Energy Mater. **2** (2019) 13.
8 S. Sugawara, T. Sato, T. Takahashi, T. Isobe, A. Nakajima, and S. Matsushita: Mater. Res. Innov. **23** (2017) 49.
9 S. Matsushita, A. Tsuruoka, Y. Kimura, T. Isobe, and A. Nakajima: Solid-State Electron. **158** (2019) 70.
10 S. Matsushita, S. Sugawara, T. Ikeda, T. Araki, H. Sekiya, H. Kohata, T. Isobe, and A. Nakajima: Chem. Lett. **49** (2020) 1013.
11 H. Sekiya, T. Isobe, A. Nakajima, and S. Matsushita: Mater. Today Energy **17** (2020) 100469.
12 T. Ikeda, H. Sekiya, H. Kohata, T. Isobe, A. Nakajima, and S. Matsushita: J. Electroanal. Chem. **895** (2021) 115413.
13 H. Kohata, B. Mei, Y. Wang, K. Mizukoshi, T. Isobe, A. Nakajima, and S. Matsushita: Energy Fuels **36** (2022) 11619.
14 L. Kavan, M. Gratzel, J. Rathousky, and A. Zukalb: J. Electrochem. Soc. **143** (1996) 394.
15 M. Freiyag, J. Teuscher, Y. Saygili, X. Zhang, F. Giordano, P. Liska, J. Hua, S. M. Zakeeruddin, J.-E. Moser, M. Grätzel, and A. Hagfeldt: Nat. Photon. **11** (2017) 372.
16 M. Steglich, T. Käsebier, M. Zilk, T. Pertsch, E. B. Kley, and A. Tünnermann: J. Appl. Phys. **116** (2014) 173503.
17 H. Savin, P. Repo, G. Gastrow, P. Ortega, E. Calle, M. Garin, and R. Alcubilla: Nat. Nanotechnol. **10** (2015) 624.
18 H. Jansen, M. Boer, J. Burger, R. Legtenberg, and M. Elwenspoek: Microelectron. Eng. **27** (1995) 475.
19 Y. Zang, C. Kong, R. S. Davidsen, G. Scardera, L. Duan, K. T. Khoo, and M. Abbott: Ultramicroscopy **218** (2020) 113084.
20 G. Scardera, S. Wang, Y. Zhang, M. U. Khan, S. Zou, D. Zhang, and M. D. Abbott: IEEE J. Photovoltaics **11** (2021) 298.
21 Y. Kanamori, S. Haida, and K. Hane: IEEJ Trans. SM **130** (2010) 92 (in Japanese).
22 A. Matsutani, K. Nishioka, and M. Sato: Jpn. J. Appl. Phys. **55** (2016) 06GH05.
23 S. Schicho, A. Jaouad, C. Sellmer, D. Morris, V. Aimez, and R. Ares: Mater. Lett. **94** (2013) 86.

24 M. Steglich, T. Käsebier, E. B. Kley, and A. Tünnermann: Appl. Phys. A **122** (2016) 836.
25 Y. Chen, C. Zhang, Z. Yi, J. Wu, Y. Zhang, L. Bian, L. Iiu, X. Ye, H. Yang, and H. Li: Sol. Energy Mater. Sol. Cells **248** (2022) 112005.
26 S. An, Y. Liao, S. Shin, and M. Kim: Adv. Mater. Technol. **7** (2022) 2100912.
27 R. Castaing: Ph. D. Dissertation, Univ. of Paris (1951).
28 K. Kato: J. Finishing Soc. Jpn. **69** (2018) 441.
29 K. Murase: The 45th Electrochemistry Workshop (2015) (in Japanese). http://www.echem.mtl.kyoto-u.ac.jp/documents/20150915o.pdf